Received: 17 April 2025 | Revised: 5 September 2025 | Accepted: 8 September 2025

DOI: 10.1002/mrm.70099

Magnetic Resonance in Medicine

TECHNICAL NOTE

Fast 3D UTE in vivo T_1 and T_2^* mapping of fast relaxing knee tissues at 3 T

Maik Rothe[1,2] | **Selina Riedel**[1] | **Anne Slawig**[1,2] | **Andreas Deistung**[1,2] | **Klaus Bohndorf**[1] | **Richard Brill**[1] | **Walter A. Wohlgemuth**[1,2] | **Alexander Gussew**[1,2]

[1]University Clinic and Outpatient Clinic for Radiology, University Hospital Halle (Saale), Halle (Saale), Germany

[2]Halle MR Imaging Core Facility (HMRICF), Halle (Saale), Germany

Correspondence
Maik Rothe, University Clinic and Outpatient Clinic for Radiology, University Hospital Halle (Saale), Ernst-Grube-Str. 40, D06120 Halle (Saale), Germany.
Email: maik.rothe@uk-halle.de

Funding information
German Research Foundation; DFG, Deutsche Forschungsgemeinschaft, Grant/Award Number: INST 271/406-1

Abstract

Purpose: UTE MR imaging captures quantitative signals in fast-relaxing tissues, enabling anatomical visualization and quantitative assessment of T_1 and T_2^* relaxation times. However, the clinical application of quantitative UTE MRI is limited by long acquisition times. Therefore, this study introduces a novel UTE-based method for T_1 and T_2^* mapping, achieving submillimeter resolution in less than 10 min.

Theory and Methods: The method employs a dual-echo acquisition for fast T_2^* mapping, augmented by an additional acquisition with different T_1 weighting. This second scan enables the computation of signal ratios between scans with different T_1-weighting. These measured signal ratios are then compared to a lookup table containing distinct ratios, corresponding to discrete T_1 values. The approach was validated in phantom solutions mimicking various T_1 and T_2^* times and applied in vivo to quantify relaxation times across different knee tissue compartments in healthy individuals.

Results: The method demonstrated its reliability for T_1 and T_2^* quantification in rapidly relaxing tissues (1–11 ms). However, it exhibited a tendency to underestimate T_2^* in skeletal muscle. This limitation arises from the chosen TEs being inadequate to capture slow signal decays. In accordance with the findings of preceding studies, this in vivo study identified three distinct T_1 categories of tissue characterized by short (adipose tissue), moderate (ligaments, tendons, and menisci), and long (skeletal muscle) T_1 values.

Conclusion: The presented technique for combined T_1 and T_2^* mapping enables relaxometry in rapidly relaxing tissues, indicating potential for advanced tissue characterization in clinical settings.

KEYWORDS

T_2^* mapping, knee joint, quantitative imaging, T_1 mapping, UTE

1 | INTRODUCTION

MRI of tendons and ligaments is limited by the rapid transverse relaxation times. Conventional sequences with TEs of several milliseconds yield only weak signals from these tissues. UTE techniques enable imaging of fast-relaxing tissues.[1–3] Quantitative UTE MRI provides access to proton density, relaxation, and magnetization transfer properties, offering insights into bound and free water fractions in collagen[4–6] and enabling detection of physiological and pathological changes due to aging, strain, or injury.[7,8]

The knee joint represents a clinically relevant target for quantitative UTE imaging owing to its complex anatomy and abundance of fast-relaxing tissues. Pathological changes in tendons,[9] ligaments,[10–13] cartilage,[14,15] and menisci[16] can be characterized by T_1 and effective T_2^* relaxation. Whereas T_2^* is sensitive to local magnetic field inhomogeneities, T_1 more directly reflects the free water content.[17] Therefore, mapping of both enables more comprehensive tissue assessment. The anterior cruciate ligament (ACL), for instance, is particularly prone to degenerative or traumatic injury.[18–20] Early detection of scarring or partial tears may improve treatment outcomes.

Recent UTE studies performed exponential fitting of multiple echoes for T_2^* mapping.[21–23] T_1 mapping via inversion recovery (IR) is accurate but time-consuming and suboptimally suited for short T_2^* tissues due to ineffective inversion. Faster but less precise alternatives include saturation recovery with variable flip angle (FA)[24,25] or variable TR.[22] Clinical adoption of UTE relaxometry is limited by long scan times, especially with 3D radial or spiral encoding. Few studies have simultaneously quantified T_1 and T_2^* in fast-relaxing knee tissues,[9,22,26] typically achieving 2 mm resolution in about 20 min.

In this study, we propose a time-efficient UTE-based method for combined T_1 and T_2^* mapping of the knee joint at submillimeter isotropic resolution. The method comprises two UTE scans: a dual-echo acquisition for T_2^* mapping and a scan with variable T_1 weighting to enable lookup table (LUT)–based T_1 quantification.[27] Validation included phantom experiments and in vivo measurements in healthy volunteers across different knee joint tissues, with comparison to literature values.

2 | THEORY

The proposed mapping protocol uses two UTE scans with different parameter settings, complemented by a low-resolution B_1^+ map (Figure 1). The first scan acquires one ultrashort echo (S_1) with minimized T_1 contrast. The second scan acquires two echoes (S_2, S_3) using parameters optimized for T_1 sensitivity and for the Ernst-angle condition in tissues with a T_1 of approximately 500 ms.

2.1 | T_2^* mapping

The spoiled gradient echo signal can be modeled as follows[28]:

$$S = S_0 \sin(\alpha)\frac{1-e^{-\frac{T_R}{T_1}}}{1-e^{-\frac{T_R}{T_1}}\cos(\alpha)}e^{-\frac{T_E}{T_2^*}}, \quad (1)$$

where S is the signal intensity, S_0 is the signal intensity at TE = 0 ms, and α is the FA.

T_2^* can be calculated by logarithmic ratio of two echoes acquired in the second scan:

$$T_2^* = \frac{TE_3 - TE_2}{\ln(S_2/S_3)}, \quad (2)$$

where S_2 and S_3 are signal intensities at ultrashort (TE_2) and moderate (TE_3), respectively. TE_3 is selected to satisfy the in-phase condition according to the scanner's operating frequency (123.256 MHz at our 3 T system), assuming a chemical shift of 3.3 ppm between water and fat.[29]

Beyond ensuring in-phase acquisition, TE_3 must also be matched to the expected T_2^* range. Long TE_3 improves accuracy for long T_2^* values but reduces it for short T_2^* and vice versa (Figure S1). Details and visualizations of TE_2/TE_3 optimization are provided in Figure S1. In this study, T_2^* mapping was evaluated for two different settings of TE_3 (2.46 ms and 4.92 ms) and compared to conventional mono-exponential fitting of three echoes (TEs = 0.03/2.46/4.92 ms).

2.2 | T_1 mapping

T_1 values are derived from two UTE measurements, S_1 and S_2, acquired with different FA and/or TR, using the signal model described in Equation 1. Because the ratio S_1/S_2 is determined by the underlying T_1 value, we constructed a LUT that maps discrete S_1/S_2 ratios to specific T_1 values within a predefined range[27] (1–4000 ms in 1 ms steps in our study):

$$\frac{S_1}{S_2} = \frac{\sin(\alpha_1)\left(1-e^{-\frac{TR_1}{T_1}}\right)\left(1-e^{-\frac{TR_2}{T_1}}\cos(\alpha_2)\right)}{\sin(\alpha_2)\left(1-e^{-\frac{TR_2}{T_1}}\right)\left(1-e^{-\frac{TR_1}{T_1}}\cos(\alpha_1)\right)}. \quad (3)$$

Accurate knowledge of the actual FAs is crucial but can be extracted from a low-resolution B_1^+ map.

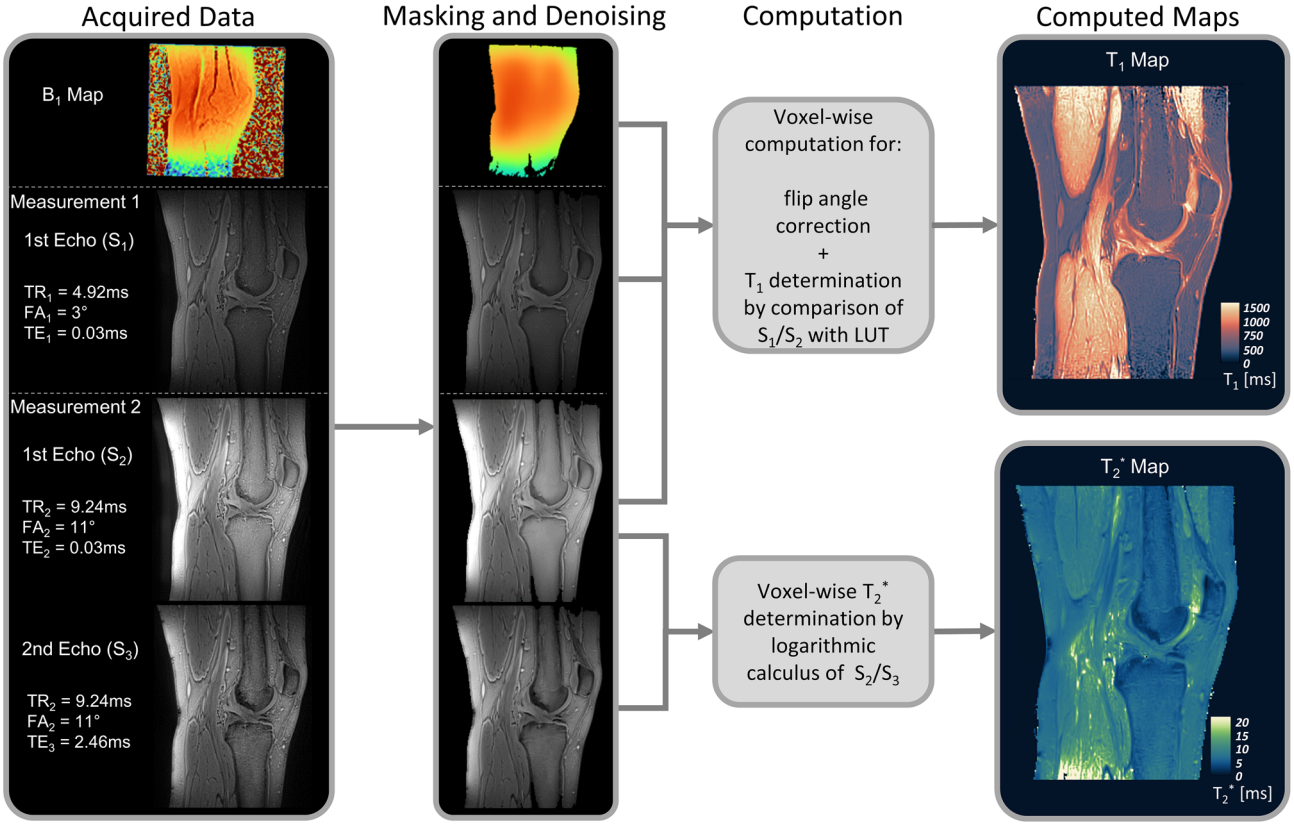

FIGURE 1 Overview of the proposed method for T_1 and T_2^* mapping, illustrated on a sagittal knee image using the Lipari and Navia color maps.[71] The left column presents the proposed acquisition scheme consisting of two UTE scans and B_1^+ mapping. In the subsequent image preprocessing, the background was removed by masking and the SNR was improved by a denoising algorithm (second column). After these steps, the T_1 and T_2^* maps were calculated (third column). The right column shows the corresponding T_2^* map (based on logarithmic calculation of S_2 and S_3) as well as the B_1^+-corrected T_1 map (based on S_1 and S_2 via LUT). Peripheral T_1 inhomogeneity in muscle (e.g., femur) may reflect transmit-field imperfections at the edge of the FOV. LUT, lookup table; S, signal intensity.

The choice of FA_1/FA_2 and TR_1/TR_2 also depends on the expected T_1 range and is constrained by the settings used for T_2^* mapping. To reduce scan time, TR_1 and TR_2 are kept as short as possible. FA_2 is selected according to the Ernst angle for tissues with $T_1 \approx 500$ ms. This leaves FA_1 as the only remaining parameter to be optimized. It must be small enough to minimize T_1 weighting across a broad T_1 range, while remaining large enough to ensure adequate SNR in the first UTE scan (S_1). Based on numerical simulations (Figure S1), $FA_1 = 3°$ was chosen as a sufficient compromise.

3 | METHODS

The proposed fast T_1 and T_2^* mapping approach was evaluated in vitro and applied in vivo in 20 asymptomatic young volunteers (14/6 female/male, 26.6 ± 6.2 years) with no history of knee trauma, pain, functional impairment, or intense sports activity. The study was approved by the local ethics committee (protocol no.: 2021–056) and conducted in accordance with the Declaration of Helsinki; written informed consent was obtained from all participants.

3.1 | Phantom construction

Two multi-compartment phantoms were constructed to mimic T_1 and T_2^* relaxation properties in knee tissues. The T_2^* phantom (seven tubes) was designed to simulate T_2^* values between 1 ms and 20 ms using 3 wt% carrageenan gels with 0.9 wt% sodium chloride and varying cornstarch concentrations ([80/70/60/50/45/40/33] wt%). Cornstarch effectively shortens T_2^* without inducing B_0 field distortions.[30–32] The T_1 phantom (10 tubes) simulated T_1 values between 300 and 1300 ms[33,34] using 3 wt% agarose gels with 0.9 wt% sodium chloride and graded concentrations of gadolinium ([300/180/140/80/60/40/30/20/12/7] μM, gadobutrol).

3.2 | Data acquisition

MRI was performed on a clinical 3 T MR scanner (Magnetom Vida, Siemens Healthineers, Erlangen, Germany) using an 18-channel transmit/receive knee coil. In vivo scans were acquired with volunteers in supine position, with knees fixated and angulated by approximately 15°.

The imaging protocol included two UTE scans with 3D stack-of-spirals readout (prototype spoiled gradient echo UTE sequence[35,36]) and a low-resolution B_1^+ map (Figure 1). Scans were performed in sagittal orientation with 0.8 mm isotropic resolution (20 µs block-pulse excitation, FOV: 198 × 198 mm^2, matrix: 256 × 256, 172 slices, slice thickness: 0.8 mm). Each slice was encoded with 512 spiral readouts (1160 µs readout, 682 samples, spectral bandwidth: 588 kHz, pixel bandwidth: 2298 Hz/pixel, TE range: 30–660 µs from k-space center to periphery).

- Measurement 1 (3:18 min): TE: 0.03 ms, TR_1: 4.92 ms, FA_1: 3°
- Measurement 2 (5:56 min): TE: 0.03/2.46/4.92 ms, TR_2: 9.24 ms, FA_2: 11°

B_1^+ mapping was performed using a low-resolution 2D multi-slice turboFLASH sequence[37,38] (TR/TE: 29660/2.56 ms, FA_1/FA_2: 8/80°, FOV: 200 × 200 mm,[2] acquisition matrix: 96 × 96, slice thickness: 2 mm). To verify suitability for FA correction, additional experiments in a large cylindrical phantom were performed using the employed B_1^+ mapping sequence (Figure S2).

As a reference for T_2^* quantification across a broad T_2^* range, the T_2^* phantom was scanned using an echo-train shifted multi-echo (ETsME) approach. Here, 22 measurements were repeated with the first echo shifted from TE_1: 30–1500 µs, while keeping the subsequent echoes constant ($TE_{2\text{-}5}$: 4.92/7.38/9.84/12.3 ms, TR: 13 ms; FA: 12°). Reference T_1 values of the T_1 phantom were obtained via inversion-prepared UTE scans (TE/TR: 0.03/4.4 ms, FA: 6°, 22 TIs: 30–8000 ms) and fitted using three free parameters.

3.3 | Data preprocessing

The low-resolution B_1^+ map was resampled and aligned to the high-resolution UTE images using the FreeSurfer package (version 7.4.0) (http://surfer.nmr.mgh.harvard.edu[39]). Subsequent processing was performed with custom Python scripts using standard libraries.[40] To mitigate FA uncertainty in fast-relaxing tissues, the B_1^+ map was polynomially smoothed and used to compute voxelwise FA correction factors. UTE images were denoised using an adaptive nonlocal means filtering algorithm[41] and affinely coregistered. Finally, subtraction images (S_2–S_3) were generated to highlight fast-relaxing tissue structures.

T_2^* reference values in phantoms were determined via monoexponential fitting of the ETsME decay. T_2^* mapping in both phantom and in vivo data was performed voxelwise using three different approaches:

I. 3TE: Three-point mono-exponential fit using TEs: 0.03/2.46/4.92 ms
II. $2TE_{2.46}$: Dual-echo computation (Equation (2)) using TE_2/TE_3: 0.03/2.46 ms
III. $2TE_{4.92}$: Dual-echo computation (Equation (2)) using TE_2/TE_3: 0.03/4.92 ms

T_1 mapping was performed via a LUT generated from simulated S_1/S_2 signal ratios corresponding to T_1 values between 1 ms and 4000 ms (Figure S1D). To account for B_1^+ inhomogeneity, separate LUTs were generated for FAs from 1° to 180° (1° steps). Each voxel's local FA was derived from the B_1^+ map and used to select the corresponding LUT. Reference T_1 values in the phantom were determined by monoexponential fitting of the IR series.

3.4 | Volumes of interest

Volumes of interest (VOIs) were manually defined using 3D Slicer (https://www.slicer.org[42]) based on subtraction images (S_2–S_3) and transferred to the parameter maps to extract VOI specific mean values of relaxation parameters.

Two circular VOIs per phantom tube were placed on matching slices (~3 pixels from the tube wall) and interpolated across slices to form 3D cylindrical VOIs.

In vivo, VOIs comprising at least 100 voxels were manually segmented for nine knee tissues by consensus of four raters (S.R., M.R., K.B., A.G.) based on sagittal, coronal, and axial views (Figure S3). Tissues included the ACL, posterior cruciate ligament (PCL), patellar tendon (PT), quadriceps tendon (QT), posterior horn of lateral meniscus (LM), bone marrow (BM), infrapatellar fat pad (IFP), subcutaneous adipose tissue (SAT), and skeletal muscle (SM). For the meniscus, tendons, and ligaments, only hyperintense voxels in subtraction images were selected to emphasize fast-relaxing components; vessels and fascia were excluded whenever possible.

3.5 | Statistical analysis

Agreement between the proposed and reference methods for T_2^* and T_1 quantification in phantoms was evaluated using Bland–Altman analysis. T_2^* values derived from the

3TE, $2TE_{2.46}$, and $2TE_{4.92}$ approaches were assessed in relation to those from ETsME series. LUT-based T_1 values were evaluated against values obtained from the IR method. Limits of agreement were defined as the mean difference ± 1.96 SD.

One-way analysis of variance with Tukey's post hoc test was used to evaluate tissue-specific differences in in vivo T_1 and T_2^* values. T_2^* assessment was primarily based on $2TE_{2.46}$ data. A separate analysis of variance tested for method-related differences in T_2^* values across tissues.

All analyses were performed using GraphPad Prism (version 10.0.0 for Windows, GraphPad Software, Boston, MA, www.graphpad.com). A p-value <0.05 was considered statistically significant.

4 | RESULTS

4.1 | Phantom experiments

As expected, T_1 and T_2^* values decreased in the phantoms with increasing gadolinium and cornstarch concentrations, respectively (Figure 2).

T_2^* values derived from all three UTE-based methods closely matched ETsME references, showing mean ± SD

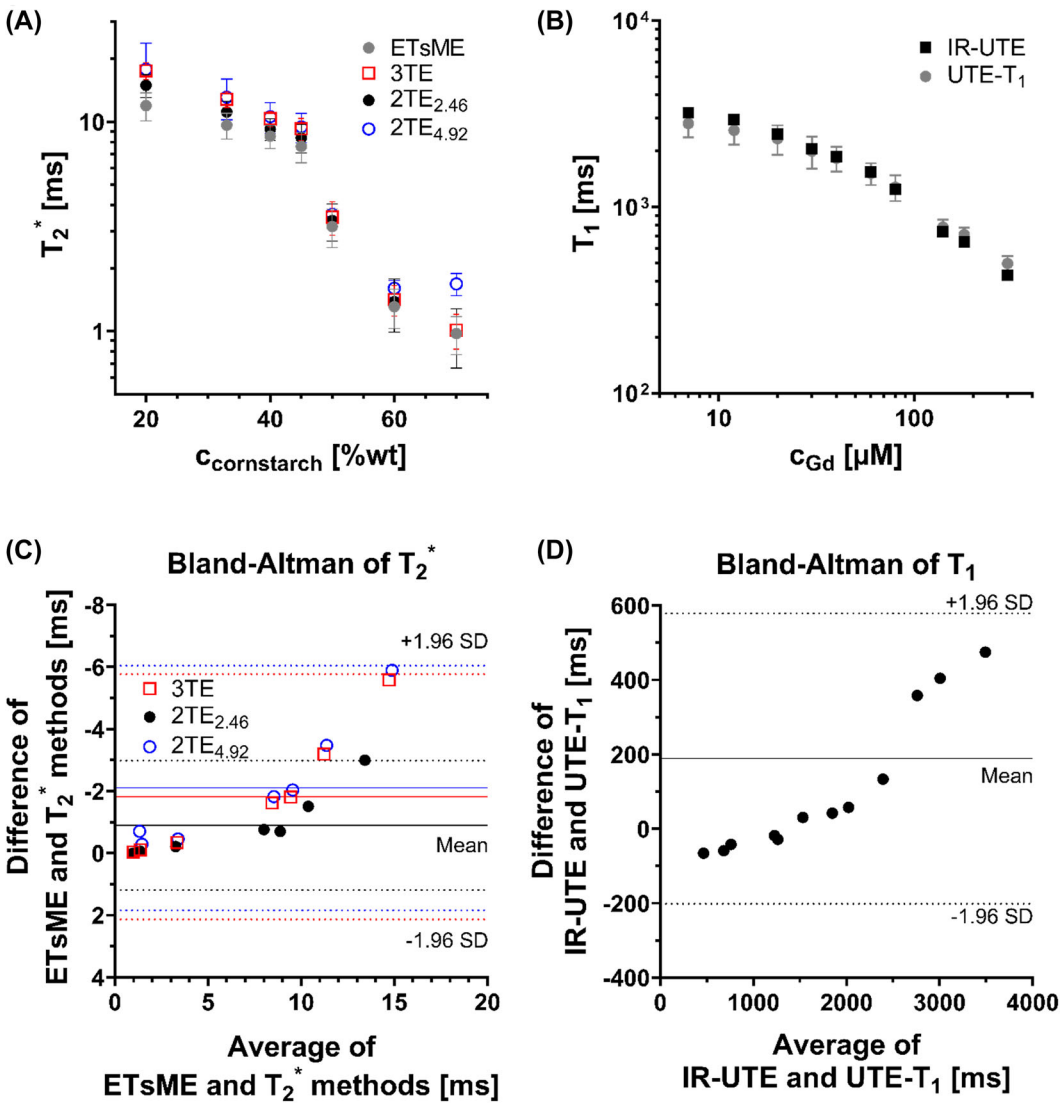

FIGURE 2 Quantitative mapping in phantom experiments. Mean T_2^* (A) and T_1 (B) values are plotted for different concentrations of cornstarch and gadolinium, respectively, for the proposed fast UTE mapping technique and the corresponding reference methods (IR-UTE for T_1 and ETsME UTE for T_2^*). The corresponding Bland–Altman plots are shown in the bottom row for T_2^* (C) and T_1 (D). The differences in (C) and (D) were calculated as reference method –mapping method. The solid and dotted lines indicate the mean and ± 1.96 SD of the differences between the reference method and the UTE-based method, respectively (red: 3TE, black: $2TE_{2.46}$, blue: $2TE_{4.92}$). ETsME, echo-train shifted multi-echo.

differences of 16% ± 10% (3TE), 9% ± 7% ($2TE_{2.46}$), and 24% ± 11% ($2TE_{4.92}$) (Figure 2A). Bland–Altman analysis (Figure 2C) demonstrated good agreement up to $T_2^* = 11$ ms; beyond this, $2TE_{4.92}$, and 3 TE increasingly overestimated T_2^*. Additionally, $2TE_{4.92}$ systematically overestimated values below 3 ms. No reliable values were obtained for $T_2^* < 1$ ms.

LUT-based T_1 values closely matched IR-UTE references (Figure 2B), with strong agreement up to $T_1 = 2500$ ms (mean difference: 2% ± 7%, maximum deviation: 9%). For $T_1 > 2500$ ms, LUT estimates exhibited reduced accuracy with a discrepancy of 13% ± 1% (Figure 2D).

4.2 | In vivo experiments

Representative UTE subtraction images and corresponding T_1 and T_2^* maps are shown in Figure 3, illustrating signal behavior and regional contrast in a healthy knee.

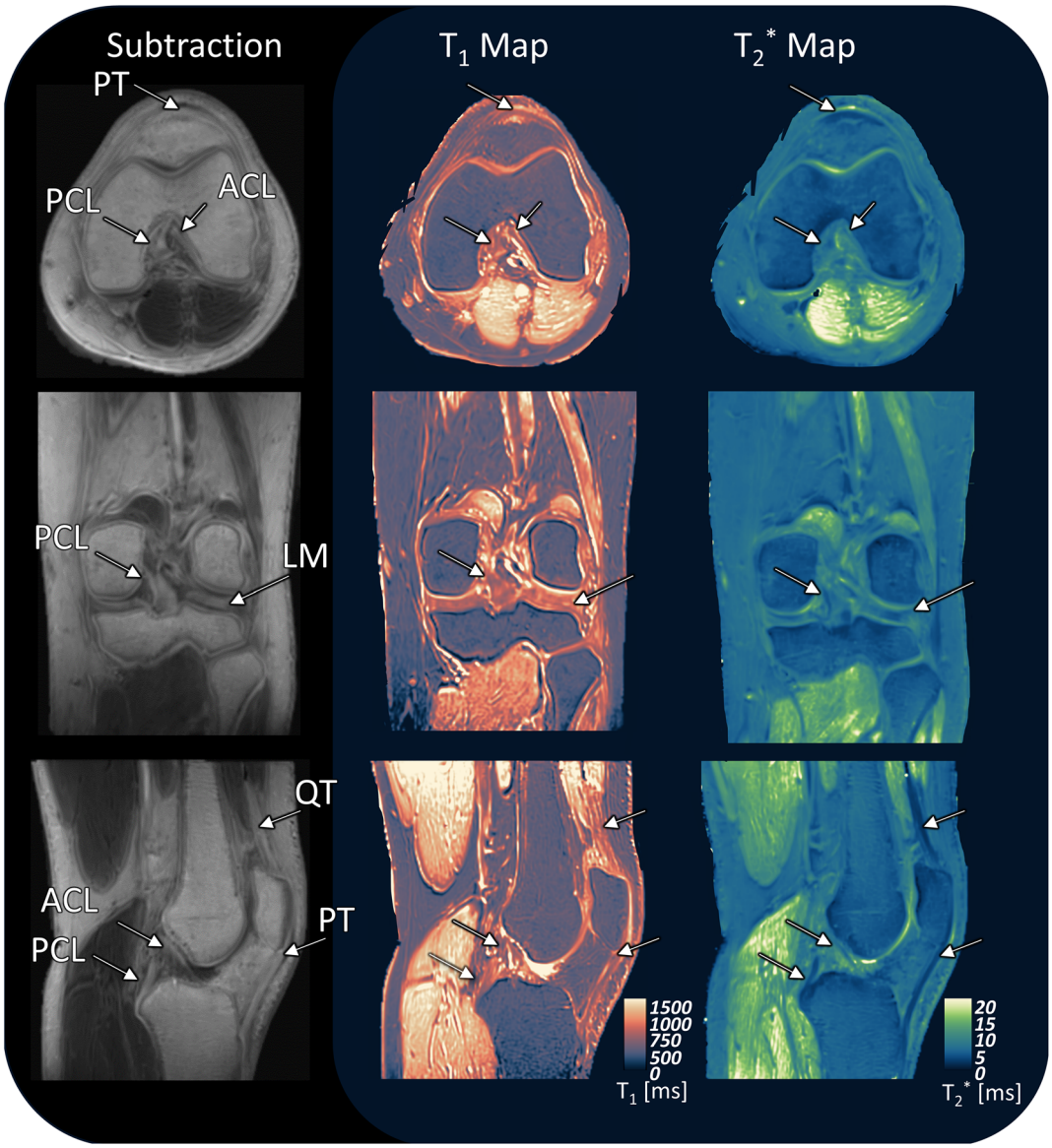

FIGURE 3 Typical images of the proposed UTE mapping method in three orientations from one volunteer. The subtraction images ($S_2 - S_3$) are shown in the left column, whereas the generated T_1 maps (displayed in Lipari colormap[71]) and T_2^* maps from the dual-echo method ($2TE_{2.46}$, displayed in Navia colormap[71]) are shown in the middle and right columns, respectively. Arrows mark the posterior horn of the LM, ACL, PCL, QT, and PT. ACL, anterior cruciate ligament; LM, lateral meniscus; PCL, posterior cruciate ligament; PT, patellar tendon; S, signal intensity; QT, quadriceps tendon.

Figure 4 and Table 1 summarize the quantitative T_1 and T_2^* values across nine examined tissue compartments, alongside literature values.

Tendons showed lower T_2^* values (3–4 ms) than ligaments (5–6 ms), with no significant differences between PT and QT or between ACL and PCL. LM T_2^* was about 8 ms. Adipose tissues—including SAT, BM, and IFP—had T_2^* values of 6–8 ms, with significantly higher values in SAT. Interindividual variability (coefficient of variation, CV) was lower in LM and adipose tissues (CV <9%) than in tendons and ligaments (CV: 10%–25%). SM T_2^* was about half of the literature values (Table 1), with considerable interindividual variability (CV: 10%–25%).

As demonstrated in the T_2^* phantom experiments, all three mapping methods yielded consistent in vivo values (Figure 4A). However, the $2TE_{2.46}$ method produced slightly elevated T_2^* values in the IFP and BM, and lower values in PT and QT.

All measured in vivo T_1 values were below 2500 ms (Figure 4B), which is within the range validated in the T_1 phantom. Tissues clustered into three characteristic T_1 groups: (i) adipose tissue with short T_1 (400 ms–500 ms,

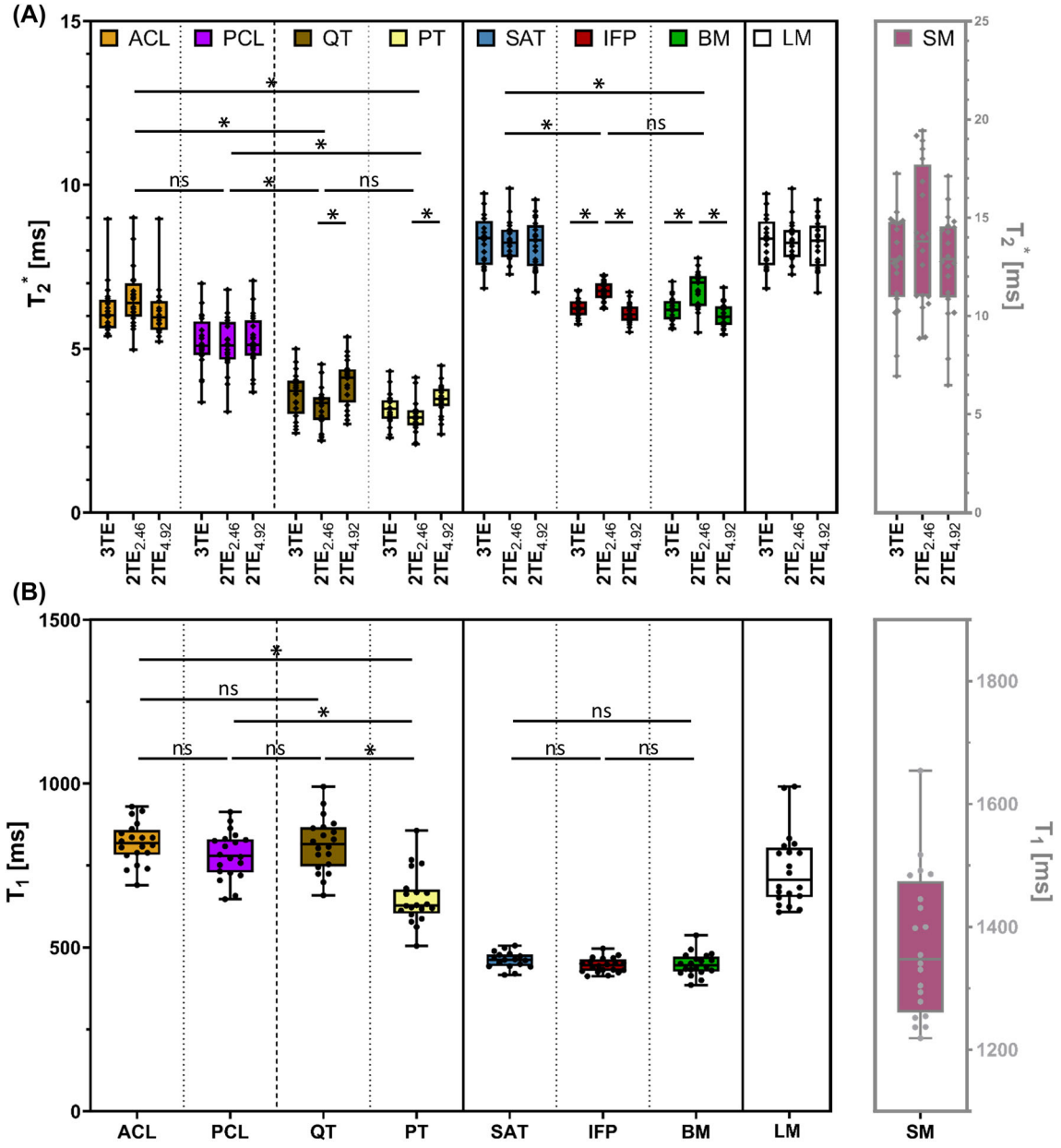

FIGURE 4 Boxplots of (A) T_2^* values from three different mapping methods and (B) T_1 values across nine knee tissue types in 20 healthy volunteers. Each circle represents an individual measurement. Statistical significance between tissue types was assessed using one-way ANOVA with Tukey's post hoc test (*$p < 0.05$). ANOVA, analysis of variance; BM, bone marrow; IFP, infrapatellar fat pad; *ns*, not significant; SAT, subcutaneous adipose tissue; SM, skeletal muscle.

TABLE 1 T_1 and T_2^* values for different tissues of the 20 knee joints of healthy volunteers obtained using the proposed imaging protocol compared to literature values.

			T_2^* [ms]			
Tissue	**T_1 [s]**	**T_1 literature [s]**	**3TE**	**$2TE_{2.46}$**	**$2TE_{4.92}$**	**T_2^* literature [ms]**
Skeletal muscle	1370 ± 120	1060–1420[33,49,61,68]	12.8 ± 2.6	14.0 ± 3.5	12.7 ± 2.7	24–32[56]
Bone marrow	450 ± 35	340–380[24,33]	6.2 ± 0.4	6.8 ± 0.6	6.0 ± 0.4	2–10.3[22,51,52,57]
Infrapatellar fat pad	450 ± 25	370–400[33,68a]	6.3 ± 0.3	6.8 ± 0.3	6.1 ± 0.4	5–12.5[22,53,54a]
Subcutaneous adipose tissue	460 ± 25	370–400[33,68]	8.3 ± 0.8	8.3 ± 0.6	8.2 ± 0.7	5–12.5[22,53,54]
Patella tendon	650 ± 85	505–660[22,49,55,61]	3.2 ± 0.5	3.0 ± 0.5	3.5 ± 0.5	1.6–6.4[22,58,60,62]
Quadriceps tendon	810 ± 85	700–800[22,49]	3.6 ± 0.7	3.2 ± 0.6	4.0 ± 0.7	1.4[22]
Posterior cruciate ligament	780 ± 75	710–840[49,55,61]	5.2 ± 0.8	5.1 ± 0.8	5.2 ± 0.8	8.3–8.8[21,55,60]
Anterior cruciate ligament	820 ± 65	740–925[49,55,61]	6.0 ± 0.5	6.3 ± 0.6	6.0 ± 0.5	9.1–16.3[11,55,60]
Lateral Meniscus	740 ± 115	600–970[49,55,61,70,73]	8.3 ± 0.8	8.3 ± 0.7	8.2 ± 0.8	5–10[3,8,16,60,73]

[a]Assuming same values for infrapatellar fat pad and subcutaneous adipose tissue.

CV: 5%–8%); (ii) tendons, ligaments, and menisci with moderate T_1 (600 ms–900 ms, CV: 8%–16%); and (iii) SM with a long T_1 (>1200 ms, CV: 9%). Within the second group, PT showed significantly lower T_1 than the ligaments ($p < 0.0001$).

5 | DISCUSSION

We present a framework for fast quantitative UTE MR imaging that enables combined T_1 and T_2^* mapping in fast-relaxing musculoskeletal tissues. All required data were acquired in under 10 min at an isotropic resolution of 0.8 mm^3. The approach can be further accelerated using techniques such as k-space undersampling[43,44] or artificial intelligence-based superresolution,[45,46] thereby further enhancing its clinical applicability. This combination of multiparametric mapping, high resolution, and short scan time distinguishes the method from previous approaches.

Typical T_2^* mapping requires ≥3 echoes and scan times of 9–20 min,[8,21,22,44,47] often at relatively low (2 mm) or anisotropic resolution, limiting accuracy in small, angled structures such as tendons or menisci due to partial volume effects. Conventional T_1 mapping using multiple TIs,[48] variable FAs,[22,49] or TRs[22] is similarly time-consuming (5–20 min) and spatially limited (~2 mm).

Despite these constraints, multi-parametric approaches—for example, multi-exponential T_2^* fits of multiple echoes—can enable more precise differentiation of tissues with distinct relaxation properties but are often impractical for routine clinical use. In contrast, our method specifically targets relevant relaxation ranges via optimized acquisition parameter combinations. The simulations and phantom experiments in this study were designed to define the sensitivity ranges and validate accuracy across different acquisition settings, such as varying TE_3 in dual-echo T_2^* mapping ($2TE_{2.46}$ vs. $2TE_{4.92}$) or adjusting FA_1 in the supplemental UTE scan for T_1 estimation.

LUT-based T_1 mapping produced accurate values up to 2500 ms, closely matching the IR-UTE reference. This confirms that simplified modeling, when paired with tailored acquisition parameters optimized for each relaxation regime, yields robust T_1 estimates in fast- as well as moderate-to-long relaxing musculoskeletal tissues.

Phantom experiments demonstrated that selecting 2.46 ms as the moderate TE in the dual-echo approach enables more accurate T_2^* values in fast-relaxing tissues (≤11 ms), with close agreement to reference ETsME fits. Using 4.92 ms led to systematic overestimation for very short T_2^* values (<3 ms), likely due to excessive signal decay exceeding the measurable dynamic range. Neither method was suitable for extremely short T_2^* (e.g., cortical bone <1 ms[50]) because signal decay was almost complete at TE = 2.46 ms.

5.1 | In vivo experiments

As in the phantom experiments, we evaluated $2TE_{2.46}$, $2TE_{4.92}$, and 3 TE T_2^* mapping in knee tissues. For meniscus and adipose tissues, T_2^* values aligned well with literature references.[3,8,56,57,16,21,22,51–55] The choice of the moderate echo significantly affected T_2^* in tendons

($p < 0.005$): $2TE_{2.46}$ yielded values closest to literature, whereas $2TE_{4.92}$ and 3 TE increasingly overestimated T_2^*, likely due to advanced signal decay at $TE_3 = 4.92$ ms. Even $2TE_{2.46}$ overestimated T_2^* in the patellar tendon compared to literature values below 3 ms.[22,58] This likely reflects the mono-exponential model's inability to resolve coexisting relaxation components—specifically collagen-bound and free water—thereby masking the fast-relaxing component of the signal in collagen-rich tissue.[59] Whereas multi-exponential models can separate such compartments,[58] they require longer scan times, limiting their clinical practicality.

Other studies reported higher T_2^* values for ACL and PCL than observed in our cohort,[11,21,55,60] likely due to different segmentation strategies: We specifically targeted fast-relaxing compartments that showed high signal in UTE subtraction images (Figure 2), whereas others analyzed entire ligament volumes, including both collagen-rich and slower-relaxing regions.[49,55,60,61]

Consistent with previous studies,[11,21,22,55,60,62] our analysis confirmed lower T_2^* values in patellar and quadriceps tendons compared to the ACL and PCL, likely due to their higher collagen content (>95% vs. < 90%).[59] Higher T_2^* in ligaments may also reflect their greater angulation relative to B_0, consistent with the "magic angle" effect.[63–67] In our cohort, tendon and ligament angles ranged between 20° and 35°, which—based on data from Wu et al.[66] on the Achilles tendon—can increase T_2^* by several milliseconds.

All applied T_2^* mapping methods underestimated skeletal muscle values due to limited sensitivity to slow-relaxing tissues,[56] necessitating longer TEs for accurate assessment.[8,21,47]

T_2^* values are anatomy- and condition-dependendent and poorly differentiate collagen-rich from fatty tissues (Figure 4). In contrast, T_1—driven by molecular mobility—better reflects tissue properties such as water and macromolecular content. Consistent with previous studies, our results delineate three tissue-specific T_1 categories (Figure 4): short T_1 in adipose tissue (high lipid content)[24,33,68]; moderate T_1 in collagen-rich ligaments, tendons, and menisci[49,55,61,69,70]; and prolonged T_1 in skeletal muscle (elevated free water content).[33,49,61,68] Notably, patellar and quadriceps tendons also differed in T_1, consistent with Krämer et al.,[22] presumably due to differences in free water and collagen content.

Adipose tissues showed higher T_1 values than literature references (Table 1), likely due to weaker T_1 weighting in S_1 for compounds with T_1 <500 ms (Figure S1C), consistent with phantom data (Figure 2B/D). Lowering FA_1 in the S_1 scan could enhance accuracy but reduce SNR, requiring systematic assessment of this tradeoff.

5.2 | Limitations

A limitation of our T_1 mapping approach is the vendor-specific 2D B_1^+ map,[38] which introduces FA uncertainty in fast-relaxing tissues. Polynomial smoothing was applied to reduce these effects, though small residual errors still may persist. Heterogeneous T_1 distributions in the FOV periphery (e.g., in bone marrow or muscles; Figure 3) likely reflect incomplete FA correction. This inaccuracy was also evident in phantom measurements, where LUT-based T_1 estimates deviated by ~10% from reference IR values near the FOV edge (Figure S2). Therefore, future work should explore B_1^+ mapping approaches more closely aligned with UTE protocols.[24,49]

Chemical shift artifacts (~1 pixel) at water–fat boundaries—particularly at muscle–fat interfaces (Figure 1) and in thin structures such as tendons, ligaments, and cortical bone—can affect T_1 and T_2^* mapping by introducing heterogeneous signal contributions in boundary voxels due to partial volume and off-resonance effects. Slightly elevated T_2^* values in tissues such as the patellar tendon may partly reflect lipid contamination. Fat suppression (e.g., Dixon, spectral saturation) could mitigate this but was not applied due to: (1) reduced efficiency from B_0 inhomogeneities, (2) prolonged scan time, and (3) limited spectral separation at short readouts (~1.16 ms). Future work should therefore develop and evaluate fat suppression techniques optimized for UTE relaxometry.

In stack-of-spirals UTE, the effective TE varies across k-space, from 30 µs centrally to >600 µs peripherally, due to the increasing duration of slice-encoding gradients. Whereas most signal is acquired at short TE, this spread can bias T_2^* estimates for ultrashort components (<2 ms), thereby reducing contrast or blurring fast-decaying signals. Thus, radial 3D UTE trajectories, which maintain uniform TE across k-space, may offer a more robust alternative for future studies.

6 | CONCLUSION

We present a fast framework for submillimeter T_1 and T_2^* mapping of fast-relaxing tissues. Whole-knee coverage was achieved in under 10 min, providing accurate estimates for T_1 up to 2500 ms and T_2^* from 1 ms to 11 ms. T_1 mapping effectively differentiated adipose, collagen-rich, and water-rich tissues. Combined T_1/T_2^* mapping improves overall tissue characterization and may enhance the assessment of small structures such as ligaments and tendons in future studies.

ACKNOWLEDGMENTS

The authors thank Siemens Healthineers for providing the 3D spiral UTE research sequence, and Thomas Benkert (MR Application Predevelopment, Siemens Healthineers) for technical support. We are also grateful to Julia Wilhelm and Clemens Mey for assistance with phantom preparation and data acquisition, and to Franziska Rhode for supporting the in vivo measurements. This study was conducted on a human research MR scanner funded by the German Research Foundation (DFG, Deutsche Forschungsgemeinschaft, INST-271/406-1-FUGG). Open Access funding enabled and organized by Projekt DEAL.

ORCID

Maik Rothe https://orcid.org/0009-0001-8533-7520
Anne Slawig https://orcid.org/0000-0003-1412-244X
Andreas Deistung https://orcid.org/0000-0002-2427-1302
Walter A. Wohlgemuth https://orcid.org/0000-0002-8076-6000
Alexander Gussew https://orcid.org/0000-0003-2300-4883

REFERENCES

1. Slawig A, Rothe M, Deistung A, et al. Ultra-short echo time (UTE) MR imaging: a brief review on technical considerations and clinical applications. *Rofo*. 2023;196:671-681.
2. Cheng KY, Moazamian D, Ma Y, et al. Clinical application of ultrashort echo time (UTE) and zero echo time (ZTE) magnetic resonance (MR) imaging in the evaluation of osteoarthritis. *Skeletal Radiol*. 2023;52:2149-2157.
3. Chang EY, Du J, Chung CB. UTE imaging in the musculoskeletal system. *J Magn Reson Imaging*. 2015;41:870-883.
4. Wehrli FW. Magnetic resonance of calcified tissues. *J Magn Reson*. 2013;229:35-48.
5. Jerban S, Ma Y, Dorthe EW, et al. Assessing cortical bone mechanical properties using collagen proton fraction from ultrashort echo time magnetization transfer (UTE-MT) MRI modeling. *Bone Rep*. 2019;11:100220.
6. Schuijf JD, Ambale-Venkatesh B, Kassai Y, et al. Cardiovascular ultrashort echo time to map fibrosis-promises and challenges. *Br J Radiol*. 2019;92:20190465.
7. Xie Y, Liu S, Qu J, Wu P, Tao H, Chen S. Quantitative magnetic resonance imaging UTE-T_2^* mapping of tendon healing after arthroscopic rotator cuff repair: a longitudinal study. *Am J Sports Med*. 2020;48:2677-2685.
8. Chu CR, Williams AA, West RV, et al. Quantitative magnetic resonance imaging UTE-T2* mapping of cartilage and meniscus healing after anatomic anterior cruciate ligament reconstruction. *Am J Sports Med*. 2014;42:1847-1856.
9. Grosse U, Syha R, Hein T, et al. Diagnostic value of T1 and T2* relaxation times and off-resonance saturation effects in the evaluation of Achilles tendinopathy by MRI at 3T. *J Magn Reson Imaging*. 2015;41:964-973.
10. Yoshimizu R, Nakase J, Okuda M, et al. Ligamentization of the reconstructed ACL differs between the intraarticular and intraosseous regions: a quantitative assessment using UTE-T_2^* mapping. *PLoS One*. 2022;17:e0271935.
11. Warth RJ, Zandiyeh P, Rao M, et al. Quantitative assessment of in vivo human anterior cruciate ligament autograft remodeling: a 3-dimensional UTE-T_2^* imaging study. *Am J Sports Med*. 2020;48:2939-2947.
12. Chu CR, Williams AA. Quantitative MRI UTE-T_2^* and T_2^* show progressive and continued graft maturation over 2 years in human patients after anterior cruciate ligament reconstruction. *Orthop J Sports Med*. 2019;7(8):2325967119863056.
13. Wilms LM, Radke KL, Latz D, et al. UTE-T_2^* versus conventional T_2^* mapping to assess posterior cruciate ligament ultrastructure and integrity-an in-situ study. *Quant Imaging Med Surg*. 2022;12:4190-4201.
14. Williams AA, Titchenal MR, Do BH, Guha A, Chu CR. MRI UTE-T_2^* shows high incidence of cartilage subsurface matrix changes 2 years after ACL reconstruction. *J Orthop Res*. 2019;37:370-377.
15. Titchenal MR, Williams AA, Chehab EF, et al. Cartilage subsurface changes to magnetic resonance imaging UTE-T_2^* 2 years after anterior cruciate ligament reconstruction correlate with walking mechanics associated with knee osteoarthritis. *Am J Sports Med*. 2018;46:565-572.
16. Williams A, Qian Y, Golla S, Chu CR. UTE-T_2^* mapping detects sub-clinical meniscus injury after anterior cruciate ligament tear. *Osteoarthr Cartil*. 2012;20:486-494.
17. Fatouros PP, Marmarou A, Kraft KA, Inao S, Schwarz FP. In vivo brain water determination by T1 measurements: effect of total water content, hydration fraction, and field strength. *Magn Reson Med*. 1991;17:402-413.
18. Spink C, Henes FO, Da Cruz L, et al. Comparison of meniscal T1rho- and T_2^*-relaxation times in professional female volleyball players and healthy controls using 3T MRI: a pilot study. *Eur J Radiol*. 2022;155:110503.
19. Best MJ, Zikria BA, Wilckens JH. Anterior cruciate ligament injuries in the older athlete. *Sports Health*. 2021;13:285-289.
20. Behzadi C, Welsch GH, Laqmani A, et al. Comparison of T_2^* relaxation times of articular cartilage of the knee in elite professional football players and age-and BMI-matched amateur athletes. *Eur J Radiol*. 2017;86:105-111.
21. Okuda M, Kobayashi S, Toyooka K, et al. Quantitative differentiation of tendon and ligament using magnetic resonance imaging ultrashort echo time T_2^* mapping of normal knee joint. *Acta Radiol*. 2021;63:1489-1496.
22. Krämer M, Maggioni MB, Brisson NM, et al. T1 and T_2^* mapping of the human quadriceps and patellar tendons using ultra-short echo-time (UTE) imaging and bivariate relaxation parameter-based volumetric visualization. *Magn Reson Imaging*. 2019;63:29-36.
23. Loegering IF, Denning SC, Johnson KM, Liu F, Lee KS, Thelen DG. Ultrashort echo time (UTE) imaging reveals a shift in bound water that is sensitive to sub-clinical tendinopathy in older adults. *Skeletal Radiol*. 2021;50:107-113.
24. Maggioni MB, Krämer M, Reichenbach JR. Optimized gradient spoiling of UTE VFA-AFI sequences for robust T_1 estimation with B_1-field correction. *Magn Reson Imaging*. 2021;82:1-8.
25. Schabel MC, Morrell GR. Uncertainty in T1 mapping using the variable flip angle method with two flip angles. *Phys Med Biol*. 2009;54:N1-N8.

26. Grosse U, Springer F, Hein T, et al. Influence of physical activity on T1 and T2* relaxation times of healthy Achilles tendons at 3T. *J Magn Reson Imaging*. 2015;41:193-201.
27. El-Sharkawy AEM, Schar M, Ouwerkerk R, Weiss RG, Bottomley PA. Quantitative cardiac 31P spectroscopy at 3 Tesla using adiabatic pulses. *Magn Reson Med*. 2009;61:785-795.
28. Haacke EM, Brown RW, Thompson MR, Venkatesan R. *Magnetic Resonance Imaging: Physical Principles and Sequence Design: Physical Principles and Sequence Design 1st ed*. Hoboken, NJ: John Wiley & Sons; 1999.
29. Stirnberg R, Brenner D, Stöcker T, Shah NJ. Rapid fat suppression for three-dimensional echo planar imaging with minimized specific absorption rate. *Magn Reson Med*. 2016;76:1517-1523.
30. Choi SG, Kerr WL. 1H NMR studies of molecular mobility in wheat starch. *Food Res Int*. 2003;36:341-348.
31. Chatakanonda P, Chinachoti P, Sriroth K, et al. The influence of time and conditions of harvest on the functional behaviour of cassava starch – a proton NMR relaxation study. *Carbohydr Polym*. 2003;53:233-240.
32. Zhang D, Mu T, Sun H. Comparative study of the effect of starches from five different sources on the rheological properties of gluten-free model doughs. *Carbohydr Polym*. 2017;176:345-355.
33. Jordan CD, Saranathan M, Bangerter NK, Hargreaves BA, Gold GE. Musculoskeletal MRI at 3.0 T and 7.0 T: a comparison of relaxation times and image contrast. *Eur J Radiol*. 2013;82:734-739.
34. Hattori K, Ikemoto Y, Takao W, et al. Development of MRI phantom equivalent to human tissues for 3.0-T MRI. *Med Phys*. 2013;40:032303.
35. Qian Y, Boada FE. Acquisition-weighted stack of spirals for fast high-resolution three-dimensional ultra-short echo time MR imaging. *Magn Reson Med*. 2008;60:135-145.
36. Mugler JI, Fielden SW, Meyer CH, et al. Breath-hold UTE lung imaging using a stack-of-spirals acquisition. In: *Proceedings of the 23rd Annual Meeting of ISMRM, 30 May to 5 June 2015, Metro Toronto Convention Centre, Toronto, ON M5V 3L9, Canada*; 2015:1476.
37. Haase A, Frahm J, Matthaei D, Hanicke W, Merboldt K. FLASH imaging. Rapid NMR imaging using low flip-angle pulses. *J Magn Reson*. 1986;67:258-266.
38. Chung S, Kim D, Breton E, Axel L. Rapid B1+ mapping using a preconditioning RF pulse with turboFLASH readout. *Magn Reson Med*. 2010;64:439-446.
39. Reuter M, Rosas HD, Fischl B. Highly accurate inverse consistent registration: a robust approach. *Neuroimage*. 2010;53:1181-1196.
40. Van Rossum G, Drake FL. *Python 3 Reference Manual*. CreateSpace; 2009.
41. Manjón JV, Coupé P, Martí-Bonmatí L, Collins DL, Robles M. Adaptive non-local means denoising of MR images with spatially varying noise levels. *J Magn Reson Imaging*. 2010;31:192-203.
42. Fedorov A, Beichel R, Kalpathy-Cramer J, et al. 3D slicer as an image computing platform for the quantitative imaging network. *Magn Reson Imaging*. 2012;30:1323-1341.
43. Donoho DL. Compressed sensing. *IEEE Trans Inf Theory*. 2006;52:1289-1306.
44. Lustig M, Donoho D, Pauly JM. Sparse MRI: the application of compressed sensing for rapid MR imaging. *Magn Reson Med*. 2007;58:1182-1195.
45. Singh D, Monga A, de Moura HL, Zhang X, Zibetti MVW, Regatte RR. Emerging trends in fast MRI using deep-learning reconstruction on undersampled k-space data: a systematic review. *Bioengineering*. 2023;10:1-44.
46. Zhou L, Wang J. An investigation into the applicability of rapid artificial intelligence-assisted compressed sensing in brain magnetic resonance imaging performed at 5 Tesla field strength. *iRADIOLOGY*. John Wiley & Sons Ltd; 2024:584-593.
47. Agergaard AS, Malmgaard-Clausen NM, Svensson RB, et al. UTE T_2^* mapping of tendinopathic patellar tendons: an MRI reproducibility study. *Acta Radiol*. 2021;62:215-224.
48. Chen J, Chang EY, Carl M, et al. Measurement of bound and pore water T1 relaxation times in cortical bone using three-dimensional ultrashort echo time cones sequences. *Magn Reson Med*. 2017;77:2136-2145.
49. Ma YJ, Zhao W, Wan L, et al. Whole knee joint T1 values measured in vivo at 3T by combined 3D ultrashort echo time cones actual flip angle and variable flip angle methods. *Magn Reson Med*. 2019;81:1634-1644.
50. Ma YJ, Jerban S, Jang H, Chang D, Chang EY, Du J. Quantitative ultrashort echo time (UTE) magnetic resonance imaging of bone: an update. *Front Endocrinol (Lausanne)*. 2020;11:567417.
51. Le Ster C, Lasbleiz J, Kannengiesser S, Guillin R, Gambarota G, Saint-Jalmes H. A fast method for the quantification of fat fraction and relaxation times: comparison of five sites of bone marrow. *Magn Reson Imaging*. 2017;39:157-161.
52. Marage L, Lasbleiz J, Fondin M, Lederlin M, Gambarota G, Saint-Jalmes H. Voxel-based mapping of five MR biomarkers in the wrist bone marrow. *MAGMA*. 2021;34:729-740.
53. Martel D, Honig S, Monga A, Chang G. Bone reports analysis of muscle, hip, and subcutaneous fat in osteoporosis patients with varying degrees of fracture risk using 3T chemical shift encoded MRI. *Bone Rep*. 2020;12:100259.
54. Andersson J, Kjellberg E, Ahlström H, Dahlgren J, Kullberg J. Original contribution MRI estimates of brown adipose tissue in children – associations to adiposity, osteocalcin, and thigh muscle volume. *Magn Reson Imaging*. 2019;58:135-142.
55. Athertya JS, Ma Y, Masoud Afsahi A, et al. Accelerated quantitative 3D UTE-cones imaging using compressed sensing. *Sensors*. 2022;22:7459.
56. Zuo CS, Sung YH, Simonson DC, et al. Reduced T_2^* values in soleus muscle of patients with type 2 diabetes mellitus. *PLoS One*. 2012;7:7-12.
57. Wang L, Wang D, Chen J. Preliminary study of confounder-corrected fat fraction and R_2^* mapping of bone marrow in children with acute leukemia. *J Magn Reson Imaging*. 2023;58:1353-1363.
58. Kijowski R, Wilson JJ, Liu F. Bicomponent ultrashort echo time T_2^* analysis for assessment of patients with patellar tendinopathy. *J Magn Reson Imaging*. 2017;46:1441-1447.
59. Fujii K, Yamagishi T, Nagafuchi T, Tsuji M, Kuboki Y. Biochemical properties of collagen from ligaments and periarticular tendons of the human knee. *Knee Surg Sport Traumatol Arthrosc*. 1994;2:229-233.
60. Wu Z, Zaylor W, Sommer S, et al. Assessment of ultrashort echo time (UTE) T_2^* mapping at 3T for the whole knee: repeatability,

the effects of fat suppression, and knee position. *Quant Imaging Med Surg*. 2023;13:7893-7909.
61. Wu M, Zhao W, Wan L, et al. Quantitative three-dimensional ultrashort echo time cones imaging of the knee joint with motion correction. *NMR Biomed*. 2020;33:e4214. doi:10.1002/nbm.4214
62. Breda SJ, Poot DHJ, Papp D, et al. Tissue-specific T_2^* biomarkers in patellar tendinopathy by subregional quantification using 3D ultrashort Echo time MRI. *J Magn Reson Imaging*. 2020;52:420-430.
63. Hänninen N, Rautiainen J, Rieppo L, Saarakkala S, Nissi MJ. Orientation anisotropy of quantitative MRI relaxation parameters in ordered tissue. *Sci Rep*. 2017;7:9606.
64. Gil R, Khabipova D, Zwiers M, Hilbert T, Kober T, Marques JP. An in vivo study of the orientation-dependent and independent components of transverse relaxation rates in white matter. *NMR Biomed*. 2016;29:1780-1790.
65. Bydder M, Rahal A, Fullerton GD, Bydder GM. The magic angle effect: a source of artifact, determinant of image contrast, and technique for imaging. *J Magn Reson Imaging*. 2007;25:290-300.
66. Wu M, Ma Y, Wan L, et al. Magic angle effect on adiabatic T1ρ imaging of the Achilles tendon using 3D ultrashort echo time cones trajectory. *NMR Biomed*. 2020;33:e4322. doi:10.1002/nbm.4322
67. Du J, Pak BC, Znamirowski R, et al. Magic angle effect in magnetic resonance imaging of the Achilles tendon and enthesis. *Magn Reson Imaging*. 2009;27:557-564.
68. Gold GE, Han E, Stainsby J, Wright G, Brittain J, Beaulieu C. Musculoskeletal MRI at 3.0 T: relaxation times and image contrast. *Am J Roentgenol*. 2004;183:343-351.
69. Krämer M, Herzau B, Reichenbach JR. Segmentation and visualization of the human cranial bone by T_2^* approximation using ultra-short echo time (UTE) magnetic resonance imaging. *Z Med Phys*. 2020;30:51-59.
70. Mittal S, Pradhan G, Singh S, Batra R. T1 and T2 mapping of articular cartilage and menisci in early osteoarthritis of the knee using 3-Tesla magnetic resonance imaging. *Pol J Radiol*. 2019;84:e549-e564.
71. Fuderer M. Color-map recommendation for MR relaxometry maps. *Magn Reson Med*. 2025;93:490-506.
72. Ziegler S, Braun H, Ritt P, Hocke C, Kuwert T, Quick HH. Systematic evaluation of phantom fluids for simultaneous PET/MR hybrid imaging. *J Nucl Med*. 2013;54:1464-1471.
73. Byra M, Wu M, Zhang X, et al. Knee menisci segmentation and relaxometry of 3D ultrashort echo time cones MR imaging using attention U-net with transfer learning. *Magn Reson Med*. 2020;83:1109-1122.

SUPPORTING INFORMATION

Additional supporting information may be found in the online version of the article at the publisher's website.

Figure S1. Simulation-based optimization of echo times and flip angles for dual-echo T_2^* and LUT-based T_1 mapping in UTE MRI. (A) Simulated gradient-echo signal decay curves for different T_2^* values. Vertical lines mark the ultrashort (0.03 ms) and the first two in-phase echoes at 3 T (2.46 ms, 4.92 ms), assuming a 3.3 ppm water–fat chemical shift at 123.256 MHz. In this study, $TE_2 = 0.03$ ms and $TE_3 = 2.46$ ms or 4.92 ms were used. (B) Ratio S_2/S_3 as a function of T_2^* for different TE_3 values (TE_2 fixed at 0.03 ms). The shaded area indicates the optimal sensitivity range: S_3 decayed by ≥25% for better discrimination of longer T_2^*, but retained >5% of S_2 to reduce noise sensitivity. (C) Simulated gradient-echo signals for ultrashort TE = 0.03 ms with varying T_1 and FA. S_2 (TR = 9.24 ms, $FA_2 = 11°$) corresponds to the T_2^* mapping scan; S_1 (TR = 4.92 ms, $FA_1 = 1–6°$) corresponds to the first UTE scan with minimized T_1 contrast. (D) Ratio S_1/S_2 versus T_1 for different FA_1 values. The dashed line marks $FA_1 = 3°$, chosen as a compromise between minimal T_1 weighting across a wide T_1 range and adequate SNR in S_1. Shaded limits indicate where S_1's T_1 weighting falls below the noise level of S_2 or where S_1 and S_2 are equal within noise.

Figure S2. Effects of B_1^+-correction on T_1-mapping. Top left: Direct comparison of T_1-mapping without B_1^+-correction, with B_1^+-correction using the dual-angle (DA) approach (as used in this study), with B_1^+-correction using the Actual Flip angle Imaging (AFI) B_1^+-mapping approach, and with a gold-standard IR-UTE-based T_1-mapping experiment. Top right: Three-plane view of the used phantom with a known T_1 of 100 ms[72] (top: axial view; middle: coronal view; bottom: sagittal view). The cylindrical phantom has a height of 20 cm and a diameter of 13 cm and consists of: 3.75 g $NiSO_4$ and 5 g NaCl per 1000 g H_2O. Six different cubic volumes (15 mm × 15 mm × 15 mm) were positioned in the isocenter along the direction of the main magnetic field. Bottom first row: B_1^+ maps obtained with the AFI (left) and DA (right) methods, displayed in % of nominal FA. The yellow box marks the cropped phantom region used for all maps and includes an overlay of a representative in vivo knee image (50% transparency) to illustrate correspondence with the in vivo field of view. Bottom second row: Corresponding T_1 maps are shown without B_1^+ correction, with DA correction, and with AFI correction. Uncorrected maps exhibit pronounced spatial inhomogeneity, which is reduced by either correction approach.

Figure S3. Visualization of manually segmented regions for the patellar tendon, quadriceps tendon, anterior cruciate ligament (ACL), posterior cruciate ligament (PCL), infrapatellar fat pad, subcutaneous adipose tissue, bone marrow, skeletal muscle and the posterior horn of the lateral meniscus. Segments are overlaid on UTE subtraction

images ($S_1 - S_2$) of a knee in axial and three sagittal views. All three planes (axial, coronal, and sagittal) were used for tissue segmentation, as exemplified for the ACL in the three images in the center column of the bottom row. Numbers indicate the planes specified by the dashed lines in the upper left corner.

How to cite this article: Rothe M, Riedel S, Slawig A, et al. Fast 3D UTE in vivo T_1 and T_2 mapping of fast relaxing knee tissues at 3 T. *Magn Reson Med*. 2026;95:693-705. doi: 10.1002/mrm.70099